Feasibility of Free Breathing 19F MRI Image Acquisition to Characterize Ventilation Defects in CF and Healthy Volunteers at Wash-in

Sang Hun Chung[1,*], **Khoi Minh Huynh, PhD**[1,*], **Jennifer L. Goralski, MD**[2,3,4], **Yong Chen, PhD**[6], **Pew-Thian Yap, PhD**[5], **Agathe S. Ceppe**[2,3], **Margret Z. Powell**[3], **Scott H. Donaldson, MD**[2,3], **Yueh Z. Lee, MD/PhD**[2,5]

[1]Department of Biomedical Engineering, University of North Carolina, Chapel Hill, USA

[2]Division of Pulmonary and Critical Care Medicine, UNC-Chapel Hill

[3]Marsico Lung Institute/UNC Cystic Fibrosis Center, UNC-Chapel Hill

[4]Division of Pediatric Pulmonology, UNC-Chapel Hill

[5]Department of Radiology and Biomedical Research Imaging Center, UNC-Chapel Hill

[6]Department of Radiology, Case Western Reserve University, Cleveland, USA

Abstract

Purpose—To explore the feasibility of measuring ventilation defect percentage (VDP) using ^{19}F MRI during free breathing wash-in of fluorinated gas mixture with post acquisition denoising and to compare these results with those obtained via traditional cartesian breath-hold acquisitions.

Methods—8 adults with cystic fibrosis (CF) and 5 healthy volunteers completed a single MR session on a Siemens 3.0T Prisma. [1]H Ultra short echo time (UTE) MRI sequences were used for registration and masking, ventilation images with ^{19}F MRI were obtained while the subjects breathed a normoxic mixture of 79% perfluoropropane and 21% oxygen. [19]F MRI was performed during breath-holds and while free breathing with one overlapping spiral scan at breath-hold for ventilation defect percentage (VDP) value comparison. The ^{19}F spiral data was denoised using a low-rank matrix recovery approach.

Results—VDP measured using ^{19}F VIBE and ^{19}F spiral images were highly correlated (r=0.84) at 10 wash-in breaths. Second breath VDPs were also highly correlated (r=0.88). Denoising greatly increased SNR (pre-denoising spiral SNR: 2.46±0.21, post-denoising spiral SNR: 33.91±6.12, breath-hold SNR: 17.52±2.08)

Conclusion—Free breathing ^{19}F lung MRI VDP analysis was feasible and highly correlated with breath hold measurements. Free breathing methods are expected to increase patient comfort and extend ventilation MRI use to patients unable to perform breath-holds, including younger subjects and those with more severe lung disease.

Corresponding author: Yueh Z. Lee, Leey@med.unc.edu, Phone: (919) 423-7195, Address: 101 Manning Drive CB #7510, Chapel Hill, NC 27599-7510.
*Author Sang Hun Chung and Author Khoi Minh Huynh contributed equally to this work

Keywords

Lung MRI; free breathing; VDP; ^{19}F; cystic fibrosis

Introduction

[19]F pulmonary MRI with fluorinated gases has been used to characterize ventilation abnormalities such as unventilated areas (ventilation defect percentages) and poorly ventilated regions (fractional lung volume with prolonged gas washout time in both cystic fibrosis (CF) and chronic obstructive pulmonary disease (COPD)[1–6]. The ^{19}F gases, including C_3F_8 and SF_6 can be mixed with oxygen to create normoxic gas mixtures. [19]F MRI has the potential to spatially measure lung function[3] at multi-slice acquisitions encapsulating the full 3D lung cavity without the need for ionizing radiation. Although hyperpolarized (HP) gas MRI approaches using [3]He [7–12] and [129]Xe[13–19] offer greater absolute signal, no hyperpolarizer is needed for ^{19}F imaging, and the signal does not decay with time. [19]F gases also make multi-breath wash-in/out studies possible due to being chemically inert and mixable with oxygen without losing its magnetic resonance behavior[4]. Multiple ^{19}F gas inhalations has been shown to be generally safe[3,20,21].

One major limitation of ^{19}F MRI with conventional sequences is the scan time required to achieve adequate signal-to-noise ratio (SNR), as most ^{19}F lung acquisitions are performed at breath-holds with an acquisition time of 5.62 to 18 seconds[4,6,22]. This limitation constrains ^{19}F lung imaging to patients able to follow commands and who are comfortable holding their breath for this duration. A much shorter acquisition time could greatly increase patient comfort and allow free breathing scans, making possible the application of ^{19}F MRI to participants unable to reliably hold their breath during image acquisition. The importance of facilitating the development of novel ventilatory biomarkers that can be used in young children cannot be understated. In the case of CF, early detection and treatment is important to prevent irreversible damage in the lungs and to allow us to study the effect of early disease interventions. However, research and development of novel therapies for children has historically been stymied by outcome measures that are impractical or impossible in young children[23–25].

Free breathing functional MRI with x-nuclei has been studied with mice lung models using hyperpolarized [129]Xe respiration-gated phase encoding[26] and using SF_6 with 5 minute acquisitions[27], both of which are not suitable for gas dynamics analysis. [19]F free breathing human lung MRI with temporal resolutions as short as 0.544 seconds[28], 0.98 seconds[29], and 2.1 seconds[4] have been achieved by Gutberlet et al. However, free breathing was applied to only the wash-out portion resulting in wash-out dynamic metrics such as time to wash-out, number of breaths to wash-out and fraction ventilation (FV), while ventilation defect percentage (VDP) was omitted[28] or measured from the static breath-hold acquisitions[4].

Analysis of VDP during multi-breath wash-in protocols has the potential to discriminate between completely unventilated lung, slowly ventilated regions, and regions with gas trapping in a way that is not feasible with single breath contrast imaging[30]. VDP has been shown to be affected by the number of contrast agent breaths, partially due to slow or

collateral ventilation[13]. Hyperpolarized methods have been traditionally performed using a single breath of tracer gas[30,31] due to difficulty to hyperpolarize large gas volumes. Oxygen (O_2) delivery with hyperpolarized gases is also a challenge due to the depolarization effect of O_2[32]. HP multi-breath wash-in lung imaging has been achieved[12] but require additional hardware for accurate on-site mixing of gas volumes and T_1 change correction. In contrast, ^{19}F gases are commercially available as pre-mixed normoxic (21% O_2) mixture that can be obtained and stored in large quantities and delivered directly to patients, making multi-breath wash-in studies logistically simpler.

This paper explores the feasibility of using a fast spiral acquisition sequence(0.45 second temporal resolution) combined with post-acquisition denoising[33] to reduce scan time while maintaining adequate SNR for the analysis of VDP during wash-in. The free-breathing acquisition method was compared to a previously published ^{19}F MRI acquisition method[6,13] where images were obtained during breath-holds. We examined the correlation of VDP determined by each approach at varying timepoints of gas intake.

Methods

Materials

MRI acquisitions were performed on a multi-nuclear capable Siemens Prisma 3.0T scanner (Siemens Medical Systems, Erlangen, Germany) and a custom, commercially available 8-channel transmit/receive ^{19}F-tuned chest coil (ScanMed, Inc., Omaha NE, model: 668SI3001). Figure 1 shows the gas delivery set-up[34], comprised of a gas reservoir and valves attached to an MR-compatible frame. The air-flow direction is controlled with one-way valves and a tight-fitting non-rebreathing mask to separate inhalation and exhalation flows. Flow-rate sensors are used to monitor inhalation/exhalation states at scan time.

8 adults with CF (ages 20–37, 6 female) and 5 healthy volunteers (ages 22–27, 3 female) contributed data to this study. Written informed consent was obtained from all participants. The study was approved by the University of North Carolina Institutional Review Board.

Acquisition

[1]H UTE MRI images were acquired with the embedded scanner body coil during a 17 second maximal inspiration breath-hold while the participant was breathing room air. Using the 3D fast low angle shot (FLASH) sequence (TE/TR, 0.05/2.42 ms; FA, 5°; resolution, 2.14×2.14 mm; slice thickness, 2.5 mm; number of slices, 103; acquisition matrix, 224×224, trajectory, spiral; interleaves, 130; spiral duration,1160 μs; slice partial Fourier, 6/8), breath-hold images were acquired at full inspiratory capacity. For the gas inhalation portion of the scan, participants breathed a mixture of 79% PFP and 21% O2 (Airgas Healthcare, Radnor, PA; used under IND 122,215). During gas wash-in, participants inhaled the PFP mixture starting with a tidal volume inspiration/expiration cycle followed by a maximal inspiration and 18 second breath-hold, as illustrated in Figure 2.

During the breath hold, a 3D Volumetric interpolated breath-hold examination (VIBE) sequence (TE/TR, 1.61/13 ms; FA, 74°; resolution of 6.25×6.25 mm; slice thickness, 15 mm; number of slices, 18; acquisition matrix, 64×64; bandwidth, 130 Hz/pixel; averages,

2; partial Fourier, 6/8) was performed; once the acquisition ended, the patient was instructed to exhale and then began next respiratory cycle (tidal inspiration/expiration then maximal inspiration with breath hold). 5 cycles were performed for the wash-in portion resulting in 5 breath-hold acquisitions (gas inhalation total: 5 deep inspirations and 5 tidal inspirations,15–20 L). The wash-out portion was collected similarly but with the participant breathing room air (not used for analysis in this study). Wash-out cycles were repeated until no ^{19}F signal was visible. More details of the approach were previously reported[6,13].

In between the breath-hold scans, a multi-shot (4 arms), 3D stack-of-spirals sequence tuned to ^{19}F was applied while the participant performed their tidal volume breath. A uniform spiral trajectory was designed and the readout time for each spiral interleaf was ~3.6 ms. A total of 12 repetitions were acquired and each repetition lasted 0.45 seconds. The participants were instructed to end breath-hold and start free breathing after 0.5 seconds had passed from the start of spiral acquisition to maintain lung inflation between VIBE and spiral acquisitions. Spatial resolution, position, and the number of slices were identical to the breath-hold VIBE acquisition. Other imaging parameters included: TE/TR, 0.48/11 ms; FA 74°; partial Fourier along the partition-encoding direction, 6/8. Similar to the VIBE acquisition, a 0.4-ms hard pulse was used in this study for volumetric excitation. The first gas intake scans are referred as VIBE_Wi2 and Spiral_Wi2 (taken after a tidal inspiration and during a deep inhalation breath-hold), the last wash-in scans are referred as VIBE_Wi10 and Spiral_Wi10 to refer to the scan time point based on the total number of wash-in inhalations (both deep and tidal).

The ^{19}F VIBE scans and ^{1}H FL3D scans were saved as DICOM images and imported to MIM (MIM 6.9.2, MIM Software, inc. Cleveland, OH) to define the whole thoracic lung cavity mask. The masks were drawn from a fusion of ^{1}H and ^{19}F VIBE, by hand and with bias towards the ^{19}F outline if inflation difference was present. The spiral scan data was exported as RAW files and reconstructed in MATLAB (MATLAB R2019b, The MathWorks, inc.) using the Michigan Image reconstruction toolbox (MIRT)[36].

Denoising

The data was denoised using low-rank matrix recovery with optimal shrinkage of singular value[37], an idea akin to Principal Component Analysis (PCA) denoising. Specifically, for each voxel, we selected a 3-by-3-by-3 block of neighboring voxels, forming a vector of voxel measurements. We then stacked the respective vectors of voxel measurements from all channels, repetitions, and timepoints to form a signal tensor, which can be reshaped to a 2-D matrix. This matrix is inherently low-rank due to signal similarity across neighboring voxels, channels, repetitions, and timepoints, as the same lung region is studied from multiple vantage points. However, the random noise obscures this low-rank structure, making the matrix full-rank. Therefore, with proper low-rank matrix recovery, we can remove the noise and reveal the underlying signal.

This approach has been proven to be effective in diffusion MRI context[33]. Note that to satisfy the random Gaussian noise assumption of the low-rank matrix recovery technique, we performed denoising for the real and imaginary part of the complex data separately. The resulting multi-coil spiral data was then combined using the adaptive reconstruction

method[38]. Lastly, the spiral scans were registered to the VIBE scans using the MATLAB functions imregtform and imtranslate rigidly using only translation.

The spiral F19 data was acquired and processed as follow:

1. Acquire 12 repetitions for 4-arm spiral data and reconstruct it using non-uniform fast Fourier transform, yielding a 5D Cartesian complex-valued data of 3 spatial dimensions (x, y, and z), channels, and repetitions.

2. Perform Mahalanobis whitening transformation for cross-channel de-correlation to ensure independent and identically distributed Gaussian noise across channels.

3. Using an overlapping sliding-block approach, a tensor of 3×3×3 voxels block across 8 channels and 12 repetitions was reshaped into a 17×96 Casorati 2D matrix for denoising. While the noisy matrix is full-rank due to noise, the actual noise-free matrix is low-rank due to correlated measurements from all channels, repetitions, and voxels in the block. We reveal this low-rank structure by mapping the matrix's singular values using an optimal shrinking function in[33,37]

Specifically, for a noisy $M \times N$ 2D matrix S, perform singular value decomposition

$$S = \sqrt{N} U \Sigma V^T$$

Where U and V are the unitary matrices containing the left and right singular vectors of S and Σ is the diagonal matrix of which diagonal elements are singular values s_1 s_2 s_3 … s_M.

The singular values are then mapped using

$$f(s) = \begin{cases} \dfrac{1}{z^2(y)y}\left(z^4(y) - \delta - \sqrt{\delta}yz(y)\right), & if \quad z^4(y) \geq \delta + \sqrt{\delta}yz(y) \\ \\ 0 \quad , & otherwise \end{cases}$$

Where $y = s/\sigma$ with noise level σ, $\delta = \dfrac{M}{N}$, and

$$z(y) = \frac{1}{\sqrt{2}}\sqrt{y^2 - \delta - 1 + \sqrt{\left(y^2 - \delta - 1\right)^2 - 4\delta}}$$

The estimated noise-free matrix is then

$$\hat{S} = \sqrt{N} U \hat{\Sigma} V^T$$

Where the diagonal matrix $\hat{\Sigma}$ has diagonal elements of $f(s_1)$, $f(s_2)$, $f(s_3)$, …, $f(s_M)$.

The noise level σ is estimated during denoising as

$$\sigma = \frac{s_{0.5}}{\sqrt{N \delta_{0.5}}}$$

Where $s_{0.5}$ is the median of all $s_1 \quad s_2 \quad s_3 \quad \cdots \quad s_M$ and $\delta_{0.5}$ is the median of the Marcenko-Pastur distribution, determined by solving

$$\int_{\delta_-}^{\delta_{0.5}} \frac{\sqrt{(\delta_+ - x)(x - \delta_-)}}{2\pi x} dx = 0.5$$

With $\delta_{\pm} = \left(\left(1 \pm \sqrt{\delta}\right)\right)^2$.

This shrinkage step was done for the real and the imaginary parts of the complex-valued data separately.

4.   Perform adaptive channel combination giving a complex 4D data of 3 spatial dimensions and the fourth for repetitions.

5.   Compute the magnitude of the complex-valued data.

6.   Select the spiral first repetition for VDP and SNR calculations.

Ventilation Defect Percentage and SNR

Regions in the lung with signal lower than the 95th percentile signal intensity[4,39] of the most posterior slice (outside the lung, representing a noise-only region) were characterized as VDP. The VIBE SNR was calculated as the ratio between the mean signal (inside the whole lung ROI, excluding VDP) over the standard deviation (taken from the most posterior slice, outside the lung). The Spiral SNR for both pre and post denoising was calculated spatially by diving voxel magnitudes by the noise standard deviation calculated by the Marchenko Pastur (MP-PCA) method[40,41,42]. The spiral SNR values are reported from the average voxel wise SNR inside the lung cavity excluding VDP regions. The VDP processing workflow is shown in Figure 3. For comparison, VDP values are taken from the first single repetition spiral scans immediately following the VIBE scans. SNR values are calculated from the last wash-in scans (Wi10).

Statistical Analysis

Analysis of variance was performed on all measured VDPs using 2-way repeated measure ANOVA and multiple comparisons were corrected with Tukey (SAS 9.4, SAS Institute Inc., Cary, NC, USA). Bland-Altman plots were generated to show difference in means. Pearson Correlation coefficients (r) were calculated using the MATLAB corrplot function (MATLAB R2019b, The MathWorks, inc.).

Results

FEV1 % predicted and SNR

FEV1 % predicted was measured for each participant prior to MRI scanning. Table 1 shows the CF/Healthy groups with the measured FEV1 % predicted and SNR values.

The ^{19}F VIBE scans yielded an average SNR of 16.93±1.80 for CF and 18.46±2.34 for the healthy group. Before the denoising procedure, 19F spiral scans had an average SNR of 2.38±0.19 for CF and 2.60±0.19 for the healthy group. The denoised ^{19}F spiral scans had an average SNR of 31.60±5.47 for CF and 37.61±5.68 for the healthy group. Figure 4 shows example slices from a VIBE acquisition (breath hold), and from spiral acquisitions before and after denoising was performed, the last bottom line shows the corresponding spiral SNR maps.

Ventilation Defect Percentage

VDP values were calculated at each breath cycle, with emphasis placed on the first scans (VIBE_Wi2, Spiral_Wi2) and after the 5th breathing cycle when the lung likely neared gas saturation (VIBE_Wi10, Spiral_Wi10). Figure 5 shows coronal slice images with VDP maps as green areas for a representative CF and healthy volunteer.

Statistical Analysis

The Pearson correlation coefficient relating the VDP from VIBE_Wi10 was highly correlated to the spiral_Wi10 VDP (r=0.84). The VDP from spiral_Wi2 was also highly correlated with both the VDPs from VIBE_Wi2 (r=0.88) and spiral_Wi10 (r=0.88). FEV1 % predicted was not strongly correlated to any measured VDP, with the highest correlations from VIBE_Wi10 (r=−0.52) and VIBE_Wi2 breath (r=−0.52).

The VDPs also showed a difference in mean values between the approaches, with the mean VDP of spiral_ Wi2 higher by 5.3 % than the mean VDP from spiral_Wi10. The mean VDP of VIBE_Wi2 was higher by 19 % over the mean VDP of VIBE_Wi10. The mean VDP of VIBE_Wi10 was lower by 1.8 % compared to the mean VDP from spiral_Wi10. The mean VDP of VIBE_Wi2 was higher by 12 % over the mean VDP of spiral_ Wi2. The differences in mean values are shown as Bland-Altman plots in Figure 6. With the exception of VIBE_Wi10 vs. spiral_Wi10 (p = 0.074), all other comparisons were found to be statistically significant with p   0.001.

VDPs at Wi2 breath were greater when compared to VDPs at the last wash-in. However, the VIBE VDPs at Wi2 were generally much higher. In Figure 7 VIBE VDPs start proportionally high before plateauing at Wi10. This effect is reduced in the spiral VDPs.

Discussion and Conclusion

Future implications

Evaluating ventilation with MRI based free-breathing approaches has been of significant interest to a number of research groups, especially given the applicability across a range of ages, and potential to eliminate sedation requirements for younger children. Though free-breathing ^{19}F studies have also been reported by other groups[4,26–29,43], our 0.45 second temporal resolution spiral ^{19}F acquisition with denoising allows free-breathing ventilation acquisition with substantial SNR improvement capable of VDP measurement. Our results suggest that ^{19}F free breathing acquisition with denoising for measuring VDP is comparable to those results obtained via cartesian VIBE breath-hold acquisitions. The significance of

these results indicates that breath-hold acquisitions could be replaced by free breathing acquisition on wash-in while maintain the ability to measure regional VDP.

With free breathing scans, participant fatigue from repeated breath holds would no longer be a limiting factor for ventilation studies; instead, the test would be constrained by the amount of gas available. Bag volumes are readily customizable, and our studies are currently performed with a 30L bag. Longer wash-in/out sessions with ^{19}F might enable the further characterization of VDP in various disease states. For example, a computed tomography (CT) study using xenon gas as contrast agent showed that in the presence of complete bronchial obstruction, unventilated areas will eventually reach signal saturation through collateral flow in 72 tidal breaths using a canine model[39]. A longer wash-in cycle might allow for additional characterization of slow-ventilating regions due to local bronchial obstruction, as compared to complete defects resulting from alveolar obstruction.

In a prior study comparing ^{19}F MRI to ^{129}Xe HP-MRI[13] in CF patients, we established that ventilation defects calculated after single breath-holds of hyperpolarized xenon were not equivalent to those assessed after multiple breaths of a perfluorinated gas. The proposed explanation is that longer exposure to a contrast gas allows for regional filling due to collateral ventilation to a partially or completely obstructed area. Thus, one might expect that additional wash-in breaths could reveal a more complete picture of the dynamic ventilatory capacity of the lung.

Removing the need for breath holds in an acquisition is anticipated to improve patient comfort, possibly improving breath size stability and compliance. We expect it will also facilitate ^{19}F scans for the pediatric population and for those unable to perform breath holds. Other MRI free breathing lung ventilation assessment methods have been recently published such as Phase-Resolved Functional Lung (PREFUL)[44–47] and a Deep Convolutional Neural Network (DCNN) based method[48]. Both methods only require ^{1}H based scans with no contrast enhancing agents. PREFUL has the added advantage of calculating perfusion and has been applied to younger CF patients in the age range of 11–16 years old[47]. However, ^{1}H MRI ventilation methods operate in the scope of single breath changes, lacking the multi-breath dynamic ventilation assessment that ^{19}F provides.

In our results, VDPs at Wi2 from the VIBE scans were higher than the first scan spiral VDPs (spiral_Wi2) by 5.3% difference in mean, which might reflect systematic 19F gas diffusion or collateral ventilation towards slow ventilated areas during the time length of the VIBE scan breath hold. Other possible causes of the lower overall VDP values from the spiral might be due to the relative decrease of noise level to the signal level due to denoising especially at voxels affected by partial volume. The spiral sequence (being sparser at the boundaries of k-space) also causes blurring which might partially explain the offset in measured VDP.

A current observation with our denoising method is that Spiral_Wi2 breath VDP values were lower compared to VIBE_Wi2. Although average signal intensity seems to be linear between the two methods, the change between signal and background noise distributions

due to denoising might be causing a discrepancy between VDP values that requires further adjustments in either denoising or VDP calculation methods.

Limitations

One limitation of this study is that our goal was to compare the two acquisition modalities while not exposing the participant to additional gas inhalation beyond what we have already studied. Therefore, we chose to run the spiral sequences in bursts of 12 repetitions in between each breath-hold acquisition. In future studies, we plan to conduct the scan with continuous spiral repetitions over multiple breaths with no interruption.

The spiral acquisition, while shortening the scan time, also introduces susceptibility to B0 inhomogeneities, Eddy currents, and gradient delay errors resulting in distortions. Many correction methods have been published[49–54] but have not yet been adapted widely by scanner manufacturers. It might be possible to achieve similar scan times using radial acquisition or acceleration methods such as GRAPPA, SENSE, or compressed sensing.

Another limitation is that SNR was calculated based on regions of interest (ROI) analysis of a ROI outside the thoracic cavity and a ROI with signal for the VIBE scans due to our group having access to only magnitude DICOM images. This approach does not provide information of spatially varying noise throughout the acquisition volume and makes it difficult for direct comparison with comparable denoising methods. The spiral SNR was calculated using the noise standard deviation from the Marchenko Pastur (MP-PCA)[41,42] denoising method. This method was used due to its ability to calculate noise standard deviation from channel combined complex MRI data without additional scans. However, the MP method assumes a gaussian noise distribution which might lead to inaccurate SNR values if the noise is not gaussian. An alternative to the ROI based SNR calculation is the pseudo multiple replica approach proposed by Robson et al.[55], which is capable of in-vivo spatial noise calculations suitable for acquisitions where patient motion or physiological noise might be an issue. Future work will use a more complete and objectively comparable SNR calculation method needed specially when comparing or optimizing denoising methods in-vivo.

Denoising

The denoising process appears to decrease the difference in VDPs between Wi2 and Wi10 values (VIBE_Wi2 - VIBE_Wi10 = 19%, spiral_Wi2 - spiral_Wi10 = 5.3%). This might be due to denoising bringing the low ventilated areas above the noise threshold. The denoising process also changes the signal and noise distributions in the images. For the VIBE data, the intensity distribution in the background follows a Chi distribution while the distribution in the lung follows a non-central Chi distribution as the data was reconstructed using the sum-of-square method[38,56]. For the spiral noise data, both before and after denoising, the intensity distributions are Rayleighian because the data was reconstructed using adaptive channel combination[38]. Note that after denoising, the noise standard deviation was significantly lower and the distributions in the background and the lung (assumed to be purely signal of interest) are distinguishable, while before denoising, there is no significant difference between them.

Low-rank matrix recovery denoising has been widely used to remove random additive noise in MR images[40,57]. Here, with the available multi-channel k-space data, our implementation[33] utilizes the similarity in multiple measurements across channels and repetitions to further improve denoising power. In case the multi-channel data is not available, a simple solution is to use variance-stabilizing-transform (VST) to Gaussianize the Rician noise in the channel-combined data prior to low-rank matrix recovery[58]. One assumption of denoising across all channels and repetitions is that the misalignment between images is not significant. In case where misalignment is prominent, one could perform registration prior to denoising or non-local block-matching to stack spatial blocks with similar structural features for denoising together[59].

Conclusion

In conclusion, this study shows the feasibility of VDP calculation with multi-breath wash-in taken during free breathing. The VDP from free-breathing acquisition was highly correlated to the VDP with breath-hold acquisition at the first wash-in scanned time point Wi2 (r=0.88) and at the last scanned wash-in time point Wi10 (r=0.84).

Supplementary Material

Refer to Web version on PubMed Central for supplementary material.

Acknowledgements:

Data Availability Statement:

Sample Matlab functions and demo script of the denoising algorithm are shared in f19denoising.yaplab.io. Revision 0.0 (SHA-1: rev 0.0, e9da98ed421443ef7126fa607a86d7e6978e9348) was used in this publication

Bibliography

1. Obert AJ, Gutberlet M, Kern AL, et al. Examining lung microstructure using 19F MR diffusion imaging in COPD patients. Magnetic Resonance in Medicine. Published online 2022.

2. Coxson HO, Leipsic J, Parraga G, Sin DD. Using pulmonary imaging to move chronic obstructive pulmonary disease beyond FEV1. Am J Respir Crit Care Med. 2014;190(2):135–144. doi:10.1164/rccm.201402-0256PP [PubMed: 24873985]

3. Couch MJ, Ball IK, Li T, et al. Pulmonary ultrashort echo time 19F MR imaging with inhaled fluorinated gas mixtures in healthy volunteers: feasibility. Radiology. 2013;269(3):903–909. doi:10.1148/radiol.13130609 [PubMed: 23985278]

4. Gutberlet M, Kaireit TF, Voskrebenzev A, et al. Free-breathing Dynamic 19F Gas MR Imaging for Mapping of Regional Lung Ventilation in Patients with COPD. Radiology. 2018;286(3):1040–1051. doi:10.1148/radiol.2017170591 [PubMed: 28972817]

5. Lee Y, Akinnagbe-Zusterzeel E, Goralski J, et al. 19F ventilation imaging of cystic fibrosis patients. Proc Int Soc Magn Reson Med. 2016;24:1607.

6. Goralski JL, Chung SH, Glass TM, et al. Dynamic perfluorinated gas MRI reveals abnormal ventilation despite normal FEV1 in cystic fibrosis. JCI Insight. 2020;5(2). doi:10.1172/jci.insight.133400

7. Kirby M, Mathew L, Heydarian M, Etemad-Rezai R, McCormack DG, Parraga G. Chronic obstructive pulmonary disease: quantification of bronchodilator effects by using hyperpolarized 3He MR imaging. Radiology. 2011;261(1):283–292. doi:10.1148/radiol.11110403 [PubMed: 21813741]

8. Fain S, Schiebler ML, McCormack DG, Parraga G. Imaging of lung function using hyperpolarized helium-3 magnetic resonance imaging: Review of current and emerging translational methods and applications. J Magn Reson Imaging. 2010;32(6):1398–1408. doi:10.1002/jmri.22375 [PubMed: 21105144]

9. Stavngaard T, Søgaard LV, Mortensen J, et al. Hyperpolarized 3He MRI and 81mKr SPECT in chronic obstructive pulmonary disease. Eur J Nucl Med Mol Imaging. 2005;32(4):448–457. doi:10.1007/s00259-004-1691-x [PubMed: 15821964]

10. Parraga G, Ouriadov A, Evans A, et al. Hyperpolarized 3He ventilation defects and apparent diffusion coefficients in chronic obstructive pulmonary disease: preliminary results at 3.0 Tesla. Invest Radiol. 2007;42(6):384–391. doi:10.1097/01.rli.0000262571.81771.66 [PubMed: 17507809]

11. Samee S, Altes T, Powers P, et al. Imaging the lungs in asthmatic patients by using hyperpolarized helium-3 magnetic resonance: assessment of response to methacholine and exercise challenge. J Allergy Clin Immunol. 2003;111(6):1205–1211. doi:10.1067/mai.2003.1544 [PubMed: 12789218]

12. Hamedani H, Clapp JT, Kadlecek SJ, et al. Regional Fractional Ventilation by Using Multibreath Wash-in (3)He MR Imaging. Radiology. 2016;279(3):917–924. doi:10.1148/radiol.2015150495 [PubMed: 26785042]

13. McCallister A, Chung SH, Antonacci M, et al. Comparison of single breath hyperpolarized 129 Xe MRI with dynamic 19 F MRI in cystic fibrosis lung disease. Magn Reson Med. 2021;85(2):1028–1038. doi:10.1002/mrm.28457 [PubMed: 32770779]

14. Ebner L, Kammerman J, Driehuys B, Schiebler ML, Cadman RV, Fain SB. The role of hyperpolarized 129xenon in MR imaging of pulmonary function. Eur J Radiol. 2017;86:343–352. doi:10.1016/j.ejrad.2016.09.015 [PubMed: 27707585]

15. Kern AL, Vogel-Claussen J. Hyperpolarized gas MRI in pulmonology. Br J Radiol. 2018;91(1084):20170647. doi:10.1259/bjr.20170647 [PubMed: 29271239]

16. Kirby M, Svenningsen S, Owrangi A, et al. Hyperpolarized 3He and 129Xe MR imaging in healthy volunteers and patients with chronic obstructive pulmonary disease. Radiology. 2012;265(2):600–610. doi:10.1148/radiol.12120485 [PubMed: 22952383]

17. Shukla Y, Wheatley A, Kirby M, et al. Hyperpolarized 129Xe magnetic resonance imaging: tolerability in healthy volunteers and subjects with pulmonary disease. Acad Radiol. 2012;19(8):941–951. doi:10.1016/j.acra.2012.03.018 [PubMed: 22591724]

18. Ouriadov A, Farag A, Kirby M, McCormack DG, Parraga G, Santyr GE. Lung morphometry using hyperpolarized (129) Xe apparent diffusion coefficient anisotropy in chronic obstructive pulmonary disease. Magn Reson Med. 2013;70(6):1699–1706. doi:10.1002/mrm.24595 [PubMed: 23359386]

19. Kanhere N, Couch MJ, Kowalik K, et al. Correlation of Lung Clearance Index with Hyperpolarized 129Xe Magnetic Resonance Imaging in Pediatric Subjects with Cystic Fibrosis. Am J Respir Crit Care Med. 2017;196(8):1073–1075. doi:10.1164/rccm.201611-2228LE [PubMed: 28245140]

20. Charles C, Moon RE, MacIntyre NR, et al. Cardio-respiratory tolerability of perfluoropropane-enhanced MRI of pulmonary ventilation. B58 LUNG IMAGING I: PHYSIOLOGIC AND CLINICAL CORRELATES. Published online 2015.

21. Halaweish AF, Moon RE, Foster WM, et al. Perfluoropropane gas as a magnetic resonance lung imaging contrast agent in humans. Chest. 2013;144(4):1300–1310. doi:10.1378/chest.12-2597 [PubMed: 23722696]

22. Charles HC, Jones RW, Halaweish AF, Ainslie MD. Parallel imaging for short breath hold times in perfluorinated gas imaging of the lung. Proceedings of the 23rd Annual Meeting of ISMRM; Toronto, Canada. Published online 2015:3984.

23. McLeod C, Wood J, Schultz A, et al. Outcomes and endpoints reported in studies of pulmonary exacerbations in people with cystic fibrosis: A systematic review. J Cyst Fibros. 2020;19(6):858–867. doi:10.1016/j.jcf.2020.08.015 [PubMed: 33191129]

24. Nissenbaum C, Davies G, Horsley A, Davies JC. Monitoring early stage lung disease in cystic fibrosis. Curr Opin Pulm Med. 2020;26(6):671–678. doi:10.1097/MCP.0000000000000732 [PubMed: 32925367]

25. Dave K, Dobra R, Scott S, et al. Entering the era of highly effective modulator therapies. Pediatr Pulmonol. 2021;56 Suppl 1:S79–S89. doi:10.1002/ppul.24968 [PubMed: 33434412]

26. Loza LA, Kadlecek SJ, Pourfathi M, et al. Quantification of ventilation and gas uptake in free-breathing mice with hyperpolarized 129 Xe MRI. IEEE transactions on medical imaging. 2019;38(9):2081–2091. [PubMed: 30990426]

27. Couch MJ, Ball IK, Li T, Fox MS, Biman B, Albert MS. 19 F MRI of the lungs using inert fluorinated gases: challenges and new developments. J Magn Reson Imaging. 2019;49(2):343–354. doi:10.1002/jmri.26292 [PubMed: 30248212]

28. Gutberlet M, Obert A, Voskrebenzev A, Klimes F, Wacker F, Vogel-Claussen J. Quantification of gas concentration and fractional ventilation using high temporal resolution MRI of pulmonary fluorinated (19F) gas washin dynamics in free breathing. Proc 26th Annual Meeting ISMRM, Paris. Published online 2018.

29. Gutberlet M, Kaireit TF, Voskrebenzev A, et al. Repeatability of regional lung ventilation quantification using fluorinated (19F) gas magnetic resonance imaging. Acad Radiol. 2019;26(3):395–403. doi:10.1016/j.acra.2018.10.021 [PubMed: 30472224]

30. Santyr G, Kanhere N, Morgado F, Rayment JH, Ratjen F, Couch MJ. Hyperpolarized gas magnetic resonance imaging of pediatric cystic fibrosis lung disease. Acad Radiol. 2019;26(3):344–354. doi:10.1016/j.acra.2018.04.024 [PubMed: 30087066]

31. Mugler JP, Altes TA. Hyperpolarized 129Xe MRI of the human lung. J Magn Reson Imaging. 2013;37(2):313–331. doi:10.1002/jmri.23844 [PubMed: 23355432]

32. Hedlund LW, Möller HE, Chen XJ, Chawla MS, Cofer GP, Johnson GA. Mixing oxygen with hyperpolarized 3He for small-animal lung studies. NMR in Biomedicine: An International Journal Devoted to the Development and Application of Magnetic Resonance In Vivo. 2000;13(4):202–206.

33. Huynh KM, Chang W-T, Chung SH, Chen Y, Lee Y, Yap P-T. Noise Mapping and Removal in Complex-Valued Multi-Channel MRI via Optimal Shrinkage of Singular Values. In: de Bruijne M, Cattin PC, Cotin S, et al., eds. Medical Image Computing and Computer Assisted Intervention – MICCAI 2021: 24th International Conference, Strasbourg, France, September 27–October 1, 2021, Proceedings, Part VI. Vol 12906. Lecture notes in computer science Springer International Publishing; 2021:191–200. doi:10.1007/978-3-030-87231-1_19

34. Charles HC, Soher BJ. Systems, methods, compositions and devices for in vivo magnetic resonance imaging of lungs using perfluorinated gas mixtures. Published online 2017.

35. Halaweish AF, Charles HC. Physiorack: an integrated MRI safe/conditional, gas delivery, respiratory gating, and subject monitoring solution for structural and functional assessments of pulmonary function. J Magn Reson Imaging. 2014;39(3):735–741. doi:10.1002/jmri.24219 [PubMed: 24123760]

36. Fessler JA. Michigan image reconstruction toolbox. Ann Arbor (MI): Jeffrey Fessler. Published online 2018.

37. Gavish M, Donoho DL. Optimal shrinkage of singular values. IEEE Trans Inform Theory. 2017;63(4):2137–2152. doi:10.1109/TIT.2017.2653801

38. Walsh DO, Gmitro AF, Marcellin MW. Adaptive reconstruction of phased array MR imagery. Magn Reson Med. 2000;43(5):682–690. doi:10.1002/(sici)1522-2594(200005)43:5<682::aid-mrm10>3.0.co;2-g [PubMed: 10800033]

39. Chae EJ, Seo JB, Kim N, et al. Collateral ventilation in a canine model with bronchial obstruction: assessment with xenon-enhanced dual-energy CT. Radiology. 2010;255(3):790–798. doi:10.1148/radiol.10090947 [PubMed: 20501716]

40. Veraart J, Fieremans E, Novikov DS. Diffusion MRI noise mapping using random matrix theory. Magn Reson Med. 2016;76(5):1582–1593. doi:10.1002/mrm.26059 [PubMed: 26599599]

41. Veraart J, Novikov DS, Christiaens D, Ades-Aron B, Sijbers J, Fieremans E. Denoising of diffusion MRI using random matrix theory. Neuroimage. 2016;142:394–406. doi:10.1016/j.neuroimage.2016.08.016 [PubMed: 27523449]

42. Does MD, Olesen JL, Harkins KD, et al. Evaluation of principal component analysis image denoising on multi-exponential MRI relaxometry. Magn Reson Med. 2019;81(6):3503–3514. doi:10.1002/mrm.27658 [PubMed: 30720206]

43. Kaireit TF, Gutberlet M, Voskrebenzev A, et al. Comparison of quantitative regional ventilation-weighted fourier decomposition MRI with dynamic fluorinated gas washout MRI and lung function testing in COPD patients. J Magn Reson Imaging. 2018;47(6):1534–1541. doi:10.1002/jmri.25902 [PubMed: 29160020]

44. Voskrebenzev A, Gutberlet M, Klimeš F, et al. Feasibility of quantitative regional ventilation and perfusion mapping with phase-resolved functional lung (PREFUL) MRI in healthy volunteers and COPD, CTEPH, and CF patients. Magn Reson Med. 2018;79(4):2306–2314. doi:10.1002/mrm.26893 [PubMed: 28856715]

45. Couch MJ, Munidasa S, Rayment JH, et al. Comparison of Functional Free-Breathing Pulmonary 1H and Hyperpolarized 129Xe Magnetic Resonance Imaging in Pediatric Cystic Fibrosis. Acad Radiol. 2021;28(8):e209–e218. doi:10.1016/j.acra.2020.05.008 [PubMed: 32532639]

46. Klimeš F, Voskrebenzev A, Gutberlet M, et al. Free-breathing quantification of regional ventilation derived by phase-resolved functional lung (PREFUL) MRI. NMR Biomed. 2019;32(6):e4088. doi:10.1002/nbm.4088 [PubMed: 30908743]

47. Munidasa S, Couch MJ, Rayment JH, et al. Free-breathing MRI for monitoring ventilation changes following antibiotic treatment of pulmonary exacerbations in paediatric cystic fibrosis. Eur Respir J. 2021;57(4):2003104. doi:10.1183/13993003.03104-2020 [PubMed: 33303537]

48. Capaldi DPI, Guo F, Xing L, Parraga G. Pulmonary Ventilation Maps Generated with Free-breathing Proton MRI and a Deep Convolutional Neural Network. Radiology. 2021;298(2):427–438. doi:10.1148/radiol.2020202861 [PubMed: 33289613]

49. Campbell-Washburn AE, Xue H, Lederman RJ, Faranesh AZ, Hansen MS. Real-time distortion correction of spiral and echo planar images using the gradient system impulse response function. Magn Reson Med. 2016;75(6):2278–2285. doi:10.1002/mrm.25788 [PubMed: 26114951]

50. Duyn JH, Yang Y, Frank JA, van der Veen JW. Simple correction method for k-space trajectory deviations in MRI. J Magn Reson. 1998;132(1):150–153. doi:10.1006/jmre.1998.1396 [PubMed: 9615415]

51. Addy NO, Wu HH, Nishimura DG. Simple method for MR gradient system characterization and k-space trajectory estimation. Magn Reson Med. 2012;68(1):120–129. doi:10.1002/mrm.23217 [PubMed: 22189904]

52. Robison RK, Devaraj A, Pipe JG. Fast, simple gradient delay estimation for spiral MRI. Magn Reson Med. 2010;63(6):1683–1690. doi:10.1002/mrm.22327 [PubMed: 20512872]

53. Tan H, Meyer CH. Estimation of k-space trajectories in spiral MRI. Magn Reson Med. 2009;61(6):1396–1404. doi:10.1002/mrm.21813 [PubMed: 19353671]

54. Bhavsar PS, Zwart NR, Pipe JG. Fast, variable system delay correction for spiral MRI. Magn Reson Med. 2014;71(2):773–782. doi:10.1002/mrm.24730 [PubMed: 23508831]

55. Robson PM, Grant AK, Madhuranthakam AJ, Lattanzi R, Sodickson DK, McKenzie CA. Comprehensive quantification of signal-to-noise ratio and g-factor for image-based and k-space-based parallel imaging reconstructions. Magn Reson Med. 2008;60(4):895–907. doi:10.1002/mrm.21728 [PubMed: 18816810]

56. Constantinides CD, Atalar E, McVeigh ER. Signal-to-noise measurements in magnitude images from NMR phased arrays. Magn Reson Med. 1997;38(5):852–857. doi:10.1002/mrm.1910380524 [PubMed: 9358462]

57. Cordero-Grande L, Christiaens D, Hutter J, Price AN, Hajnal JV. Complex diffusion-weighted image estimation via matrix recovery under general noise models. Neuroimage. 2019;200:391–404. doi:10.1016/j.neuroimage.2019.06.039 [PubMed: 31226495]

58. Ma X, U̇ urbil K, Wu X. Denoise magnitude diffusion magnetic resonance images via variance-stabilizing transformation and optimal singular-value manipulation. Neuroimage. 2020;215:116852. doi:10.1016/j.neuroimage.2020.116852 [PubMed: 32305566]

59. Coupe P, Yger P, Prima S, Hellier P, Kervrann C, Barillot C. An optimized blockwise nonlocal means denoising filter for 3-D magnetic resonance images. IEEE Trans Med Imaging. 2008;27(4):425–441. doi:10.1109/TMI.2007.906087 [PubMed: 18390341]
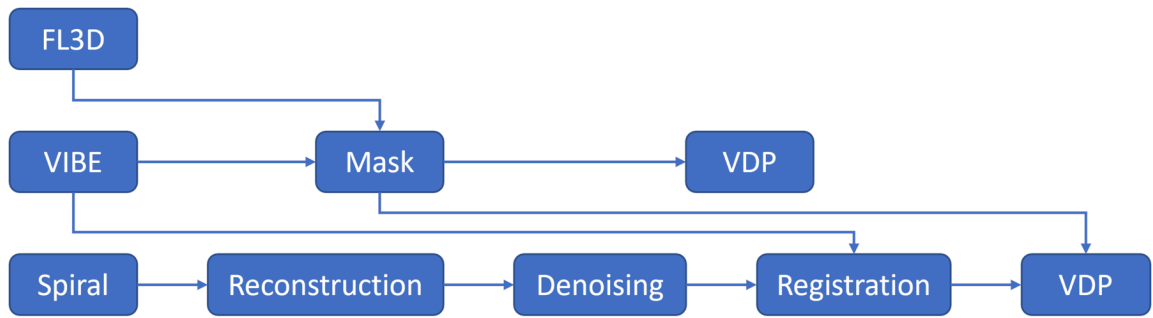
Figure 1.
Experimental set-up and gas apparatus[34,35]
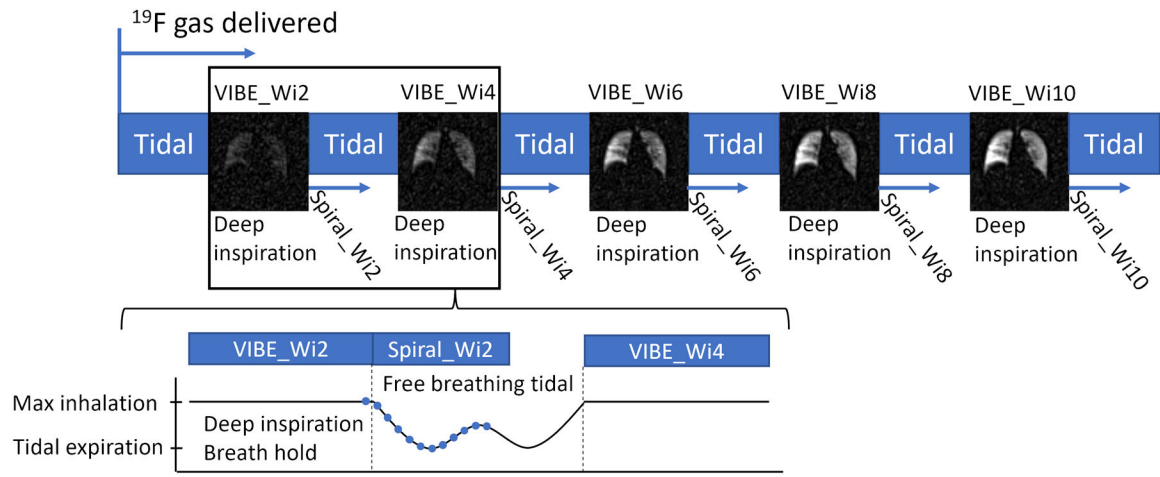
Figure 2.
Acquisition method showing 5 deep inspiration breath holds, 5 tidal inspirations, and spiral timing at wash-in, Acquisitions taken from the second and 10th inhalations (first and 5th deep inspiration breath holds) were used in the analysis of VDP. The 12 spiral repetitions are illustrated as solid circle markers, with the first spiral repetition being taken while the participant was still in breath-hold.
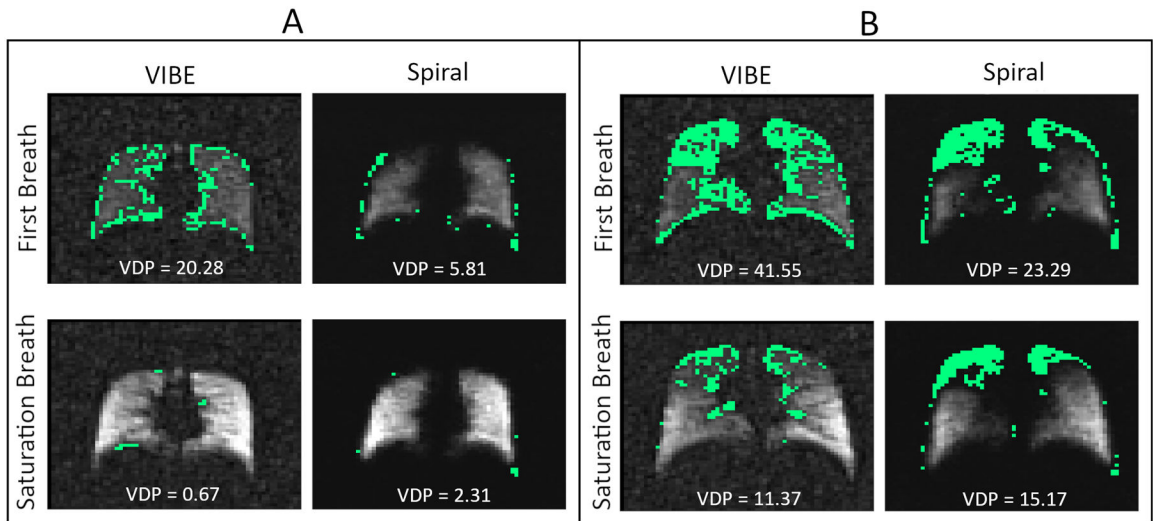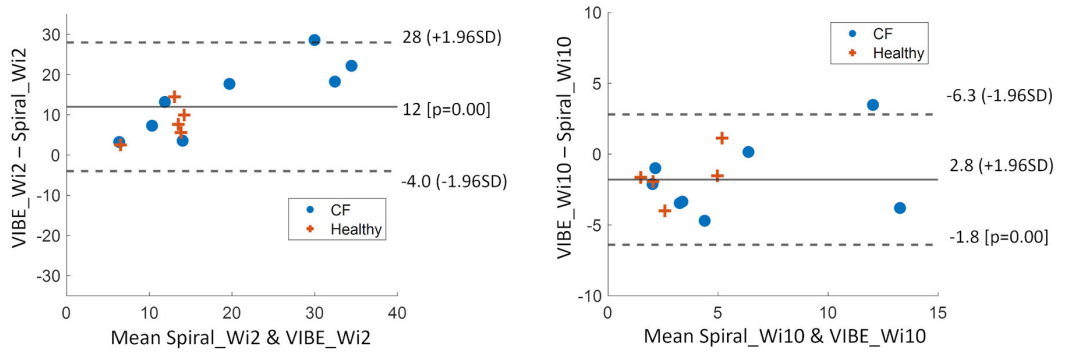
Figure 3.
Processing workflow, arrows show the inputs for each processing step. A single mask is used to calculate VDP for VIBE and Spiral acquisitions
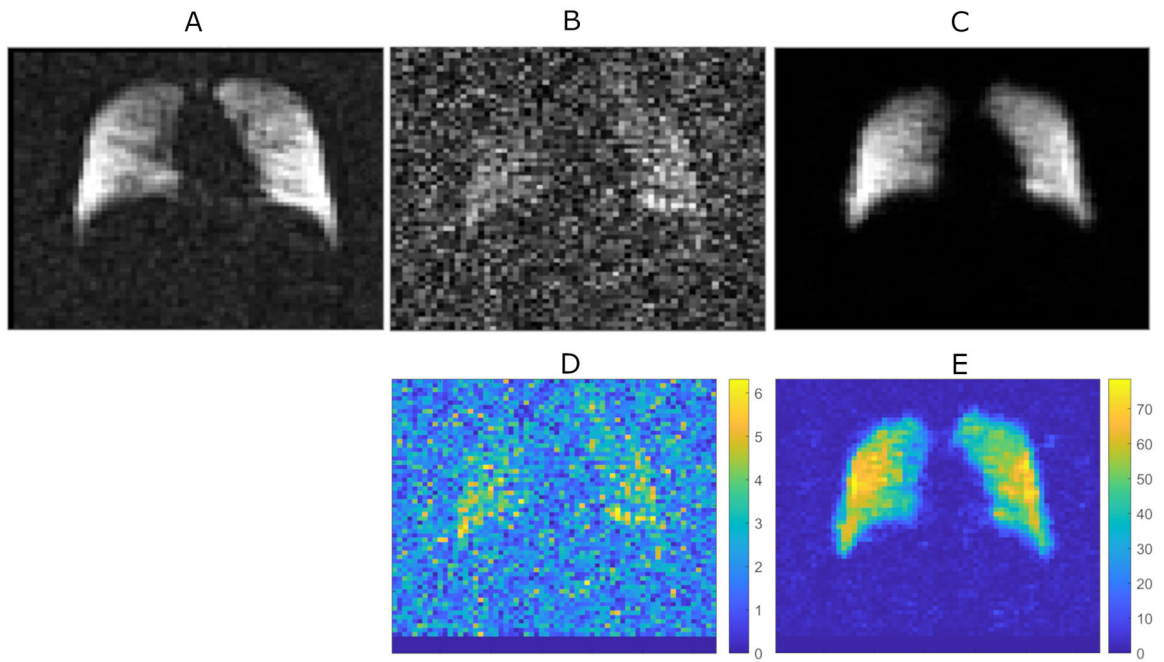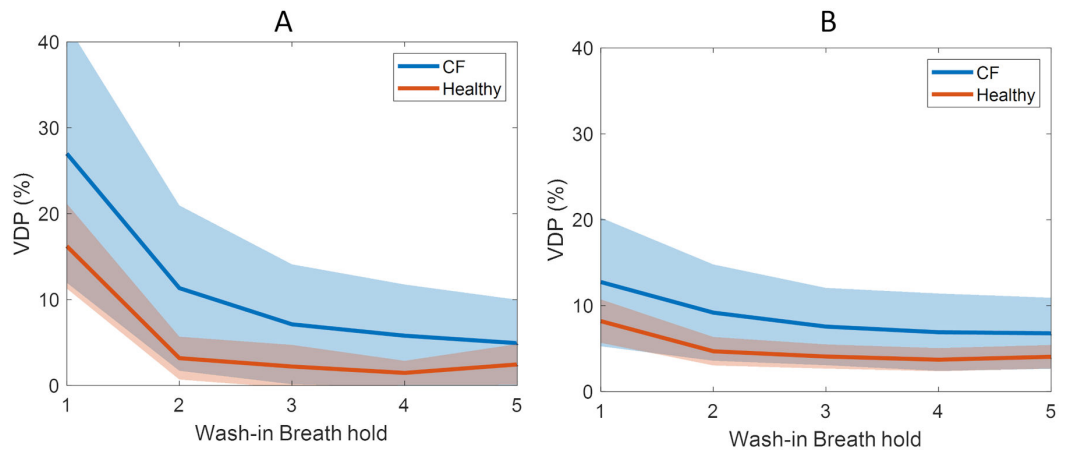
Figure 4.
Coronal slices of a healthy participant at the last wash-in scans, (A) VIBE_Wi10 at breath hold, (B) Spiral_Wi10 not denoised, (C) Spiral_Wi10 denoised, (D) Spiral_Wi10 SNR not denoised, (E) Spiral_Wi10 SNR denoised

Figure 5.
(A) Healthy participant, (B) patient with CF. VDPs are shown at the bottom of each image

Figure 6.
Bland-Altman plots between VDPs of VIBE_Wi2 & Spiral_Wi2 and VIBE_Wi10 & Spiral_Wi10, makers show CF status (solid circles: CF, orange +: Healthy)

Figure 7.
Graphs showing the relationship between average VDP and breath scan for all patients. (A) VIBE scans, (B) first repetition spiral scans for CF and healthy groups. Shaded areas show ± 1 standard deviation

Table 1.

Study Population FEV1 % predicted and SNR values

CF		SNR			Healthy		SNR		
Patient	**FEV1 % predicted**	**VIBE**	**Spiral not denoised**	**Spiral denoised**	**Patient**	**FEV1 % predicted**	**VIBE**	**Spiral not denoised**	**Spiral denoised**
1	106	16.86	2.54	36.14	9	98	17.92	2.71	41.44
2	99	17.72	2.52	35.06	10	88	19.21	2.63	40.62
3	92	17.72	2.54	38.49	11	92	19.82	2.63	36.22
4	94	14.95	2.26	26.79	12	110	20.68	2.74	41.53
5	74	13.73	2.18	25.2	13	116	14.68	2.27	28.23
6	103	19.28	2.61	36.62					
7	106	18.27	2.17	26.24					
8	64	16.93	2.24	28.28					
mean	92.25	16.93	2.38	31.60	mean	100.8	18.46	2.60	37.61
st. dev	15.46	1.80	0.19	5.47	st. dev	11.88	2.34	0.19	5.68